A Simple Element for Aeroelastic Analysis of Undamaged and Damaged Wings

Rakesh K. Kapania* and Francois Castel†
Virginia Polytechnic Institute and State University, Blacksburg, Virginia

A one-dimensional finite element has been developed to study the aeroelastic behavior of wings of arbitrary geometry and material properties distribution ranging from beam plates to builtup box structures reinforced by stringers. The formulation takes into account the effect of transverse shear and the bending-stretching coupling inherent to unsymmetric composite structures and allows for unsymmetric cross sections. A modified aerodynamic strip theory along with the V-g method is used to solve the flutter equations. The formulation has been evaluated by solving a large number of problems available in the literature. An introductory study of the bending-stretching coupling introduced by unsymmetry and damage has been conducted. It was found that the unsymmetry can have a positive or a negative influence on the aeroelastic behavior of the structure and that this influence vanishes rapidly with a decrease in coupling. It is concluded that the unsymmetry of aeroelastic structures should be considered both during the tailoring process as an added degree of design freedom and during damage tolerance assessment.

Introduction

COMPOSITES are increasingly being used in the aerospace industries. While the main driving force behind their increasing use has been their stiffness, strength and low weight, fiber reinforced materials have another property that can be described as either an advantage or an inconvenience: anisotropy. A domain in which this anisotropy has had radical effects is aeroelasticity, which can be defined as the study of the interaction among aerodynamic, elastic, and inertia forces. The most significant aeroelastic phenomena affecting aircraft structures are divergence, flutter, and control reversal.

For most earlier designs, flutter would usually occur at a lower airspeed than divergence and was therefore given more attention. This situation changed in the late 40's with the advent of the jet engine and the first incursions into the transonic speed range. It was found that the best way to reduce the high transonic drag buildup was to sweep the wing relative to the airflow. However, the divergence speed drops dramatically for even slight forward sweep angles because of what is known as "wash-in." The spanwise bending of a forward swept wing induces an increase in the local streamwise angle of attack, resulting in an increase in aerodynamic loads and thus more bending, etc. A swept-back wing experiences an opposite, or wash-out, effect. The only known cure for the wash-in of metallic wings is to increase the bending stiffness by adding a large quantity of material, resulting in an unacceptable increase in structural weight. As a result, high performance aircraft have had their wings swept back for the last 40 years. Only a handful of forward swept designs have flown, most of them adopting this configuration for nonaerodynamic reasons.

Renewed interest in the forward swept wings was prompted by the advent of modern laminated composite materials and the development of aeroelastic tailoring, the optimization of a structure's material properties to achieve a desired aeroelastic response. Krone[1] showed that the divergence instability could be eliminated for certain classes of forward swept wings without any weight penalty compared to an equivalent sweptback design. This is because, to eliminate divergence, it is only required to reduce the wash-in, and not necessarily to increase the wing stiffness. Weisshaar[2] used the Classical Lamination Theory and strip aerodynamics to derive an analytical model for the mechanisms involved. A number of analytical and wind tunnel investigations confirmed these results and culminated in the current flight testing of the Grummann X-29A forward swept wing demonstrator.

The work of Eastep, Venkayya, and Tishler,[3] which investigates the influence of damage on the divergence speed of a forward swept composite wing, is of special interest here. This work was motivated by the findings by Starnes and Haftka[4] that optimized composite structures may be more vulnerable to damage than their metallic counterparts.

Almost all of the previous studies have considered symmetrically laminated structures. They can furthermore be divided in two broad classes: either an analytical solution, applicable only to the particular problem being investigated, was developed, or, large, highly sophisticated aeroelastic optimization codes were used. There seems to be a need for a simple and efficient method to analyze a wide range of configurations, featuring unsymmetric laminations. This is the objective of this study.

The finite element method was selected for its flexibility, and a one-dimensional formulation was chosen for its simplicity. The structural model used in this study is an extension of a previous work by Kapania and Raciti[5], who developed a one-dimensional finite element for the analysis of unsymmetrically laminated uniform beams including shear deformation. Coupled with the aerodynamic model, it allows for the aeroelastic analysis of wings of arbitrary lamination, cross section, planform, and sweep distribution ranging from beam plates to builtup structures combining curved laminated cover skins, axial stringers, and shear webs.

Although there is a considerable interest in studying the damage mechanisms of advanced composite materials, very little has been published other than Ref. 3 concerning the influence of damage on the aeroelastic properties of composite wings. Because the performance of such wings depends on directional coupling as well as stiffness, they could be affected by damage in a different manner from the isotropic wings. Moreover, damage may introduce asymmetry and thus bend-

Received Oct. 25, 1988; presented as Paper 89-CP-1186 at the AIAA/ASME/ASCE/AHS/ACS 30th Structures, Structural Dynamics, and Materials Conference, Mobile, AL, April 3-5, 1989; revision received May 5, 1989.

*Assistant Professor, Aerospace and Ocean Engineering. Member, AIAA.

†Graduate Research Assistant, presently with the Composites Division, E.I. DuPont de Nemours and Co.

ing-stretching coupling in the structure, which may further modify its behavior. Some effects of such an asymmetry, introduced either by design or by damage, are studied here using highly idealized models, and results for a more complex double swept design representative of current forward swept wings are presented.

Structural Model

The wing is modeled as a beam of arbitrary cross-section distribution using a displacement-based finite element formulation. The builtup structure consists of curved top and bottom laminated skins, four webs, and eight stringers arranged in the manner shown in Fig. 1. The webs are assumed to carry the transverse shear stresses only, and the stringers are modeled as isotropic trusses capable of carrying only axial stresses. The properties of any web or stringer can be set to zero, and no membrane type assumption is made concerning the behavior of the skins so that a wide range of structures can be analyzed, from beam plates to monocoque box beams to fully builtup structures. Transverse shear is included in the formulation as is a correction factor to account for warping restraints induced by the boundary conditions. Both chord and thickness tapers are included, and the sweep angle of the wing may vary along the span.

The Beam Element

A one-dimensional beam element with 24 degrees of freedom is used. The 12 degrees of freedom at each of the two end nodes are the axial displacement u and its derivative $u' = \frac{du}{dx}$; the transverse deflection due to bending w_b and its derivative $\theta_b = w'_b$; the transverse deflection due to shear w_s and its derivative θ_s; the twist angle τ and its derivative τ'; the inplane shear β and its derivative β'; and the lateral deflection due to bending v and its derivative v'.

The element cartesian coordinate system has its x-axis running along the span of the beam, the y-axis running chordwise towards the trailing edge, and the z-axis running along the beam thickness, positive up. The origin is at node 1 on the midchord line, in the plane of the section geometric centroid, whose position is computed internally by the program. A second element coordinate system, ξ-ζ-z, is used to perform Gaussian numerical integration. It differs from the first system only in having the spanwise coordinate running from -1 at node 1 to $+1$ at node 2 and the chordwise coordinate running from -1 at the leading edge to $+1$ at the trailing edge. Both systems are described in Fig. 1.

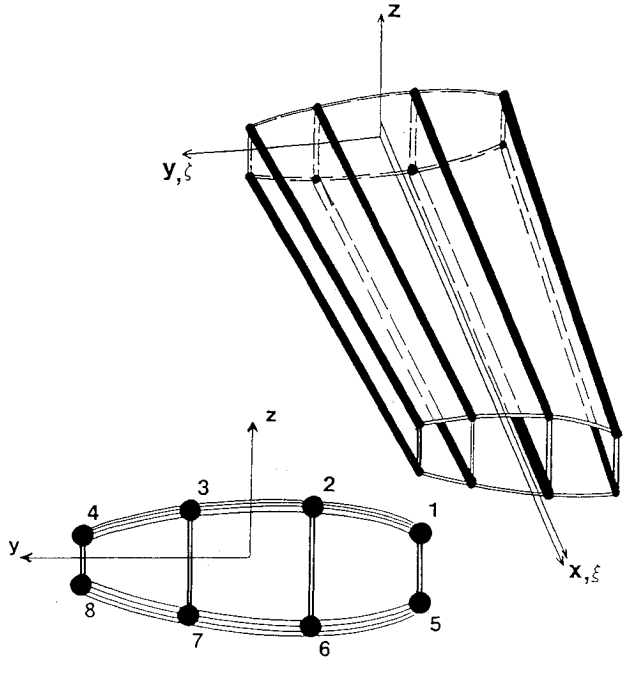

Fig. 1 Builtup wing structure and section geometry.

Each end section of the beam is defined by four pairs of section nodes as shown in Fig. 1. The pairs are located at the leading and trailing edges of the box and at two intermediate positions specified by the user. They define the value of the chord and the shape of the middle surface of the two cover skins: The middle surface of the top cover is represented by a cubic polynomial passing through the four top nodes. A similar procedure is followed to model the shape of the bottom cover. The nodes are numbered from 1 to 8 as shown in Fig. 1.

A web joins the top and bottom node of each pair of section nodes, and a stringer is located at each node. The skins are made of an arbitrary number of layers of orthotropic materials oriented at arbitrary angles from the x-axis. The thickness of the webs and skin layers as well as the stringer areas are constant within an element. The section nodes coordinates, referred to in this development as (y_i, z_i), $i = 1, \ldots, 8$, vary linearly from one end of the element to the other and are thus linear functions of x to allow for both chord and thickness taper.

The deflection behavior of the beam element is described by the displacement functions $u(x)$, $w_b(x)$, $w_s(x)$, $\tau(x)$, $\beta(x)$, and $v(x)$ in terms of the nodal displacements and their derivatives which are interpolated through Hermitian polynomials. The in-plane strains are written in terms of the previously defined displacements using the classical engineering beam theory assumptions. The slope of the cover skins is assumed to be small so that the strain components in the plane tangent to the skin do not differ significantly from the in-plane strains for the beam, that is, the strain components in the x-y plane.

A discussion of the lateral bending deflection is in order here. This degree of freedom is introduced to account for the non-symmetry of the structure caused by the arbitrary shape of the wing skin and the presence of stringers and webs. The principal axes of the beam cross section are in general not parallel to the y- and z-element coordinate axes, and a bending load in the z-axis induces a lateral deflection v in the y-axis.

The in-plane strains then are

$$\epsilon_x = \epsilon_x^0 + y\kappa_x^v + z\kappa_x^w \tag{1a}$$

$$\epsilon_y = \epsilon_y^0 + z\kappa_y \tag{1b}$$

$$\gamma_{xy} = \gamma_{xy}^0 + z\kappa_{xy} \tag{1c}$$

where ϵ_x^0, ϵ_y^0, γ_{xy}^0 are the strains at $y = z = 0$, and κ_x, κ_y and κ_{xy} are the curvatures. In the case of the beam ϵ_y^0, amd κ_y can be expressed in terms of the other strains. The relevant strains and curvatures are related to the degrees of freedom and are given in detail in Ref. 6. After interpolating the various displacements in terms of the nodal degrees of freedom, the strain-displacement relations can be expressed as

$$\{\epsilon^0\} = [B]\{q\} \tag{2}$$

where $\{\epsilon^0\} = \{\epsilon_x^0, \epsilon_y^0, \gamma_{xy}^0, \kappa_x^w, \kappa_{xy}, \gamma_{xz}, \kappa_x^v\}^t$ is the strain vector and $\{q\}$ is the nodal displacement vector.

The top and bottom covers of the box are analyzed as a single laminate, which is assumed to be in a state of plane stress. The local bending of the skins is neglected. Rewriting Eq. (1) in matrix form, we get at any point of coordinates (y,z) of a cross section

$$\{\epsilon\} = \begin{Bmatrix} \epsilon_x \\ \epsilon_y \\ \gamma_{xy} \end{Bmatrix} = [H]\{\epsilon^0\} \tag{3}$$

where the matrix $[H]$ is given in Ref. 6. The stress-strain rela-

tions are given as

$$\{\sigma\} = \begin{Bmatrix} \sigma_x \\ \sigma_y \\ \tau_{xy} \end{Bmatrix} = [\bar{Q}]\{\epsilon\} \tag{4}$$

where $[\bar{Q}]$, the local transformed reduced stiffness matrix, is a function of the material properties and fiber orientation angle.

Substituting Eq. (4) into Eq. (3) yields

$$\{\sigma\} = [\bar{Q}][H]\{\epsilon^0\} \tag{5}$$

The resultant forces acting on a cross section are now defined as

$$\{N\} = \int_{-\frac{b}{2}}^{\frac{b}{2}} \int_{z_b}^{z_t} [H]^t \{\sigma\} dz dy \tag{6}$$

where b is the chord of the beam, z_b is the z-coordinate of the bottom surface of the beam, and z_t is the z-coordinate of the top surface of the beam. Substituting Eq. (5) into Eq. (6) yields

$$\{N\} = \left[\int_{-\frac{b}{2}}^{\frac{b}{2}} \int_{z_b}^{z_t} [H]^t [\bar{Q}] [H] dz dy \right] \{\epsilon^0\} \tag{7}$$

Thus

$$\{N\} = [DL]\{\epsilon^0\} \tag{8}$$

with matrix [DL] given as follows.

$$[DL] = \begin{bmatrix} A_{11} & A_{12} & A_{16} & B_{11} & B_{12} & B_{16} & YA_1 \\ A_{12} & A_{22} & A_{26} & B_{12} & B_{22} & B_{26} & YA_2 \\ A_{16} & A_{26} & A_{66} & B_{16} & B_{26} & B_{66} & YA_6 \\ B_{11} & B_{12} & B_{16} & D_{11} & D_{12} & D_{16} & YB_1 \\ B_{12} & B_{22} & B_{26} & D_{12} & D_{22} & D_{26} & YB_2 \\ B_{16} & B_{26} & B_{66} & D_{16} & D_{26} & D_{66} & YB_6 \\ YA_1 & YA_2 & YA_6 & YB_1 & YB_2 & YB_6 & YD \end{bmatrix} \tag{9}$$

The A, B and D are defined by analogy with the Classical Lamination Theory as

$$A_{ij} = \int_{-\frac{b}{2}}^{\frac{b}{2}} \sum_{k=1}^{N+1} (z_k - z_{k-1}) \bar{Q}_{ij}^k dy$$

$$B_{ij} = \int_{-\frac{b}{2}}^{\frac{b}{2}} \frac{1}{2} \sum_{k=1}^{N+1} (z_k^2 - z_{k-1}^2) \bar{Q}_{ij}^k dy \tag{10a}$$

$$D_{ij} = \int_{-\frac{b}{2}}^{\frac{b}{2}} \frac{1}{3} \sum_{k=1}^{N+1} (z_k^3 - z_{k-1}^3) \bar{Q}_{ij}^k dy \qquad i,j = 1,2, \text{ and } 6 \tag{10b}$$

and the terms pertaining to the lateral bending deflections are

$$YA_j = \int_{-\frac{b}{2}}^{\frac{b}{2}} y \sum_{k=1}^{N+1} (z_k - z_{k-1}) \bar{Q}_{ij}^k dy \tag{11a}$$

$$YB_j = \int_{-\frac{b}{2}}^{\frac{b}{2}} \frac{y}{2} \sum_{k=1}^{N+1} (z_k^2 - z_{k-1}^2) \bar{Q}_{ij}^k dy \tag{11b}$$

$$YD = \int_{-\frac{b}{2}}^{\frac{b}{2}} y^2 \sum_{k=1}^{N+1} (z_k - z_{k-1}) \bar{Q}_{11}^k dy \qquad j = 1,2, \text{ and } 6 \tag{11c}$$

where n is the total number of plies, and z_k is the coordinate of the top surface of the kth ply, numbered from the top down. The summation goes from 1 to $n+1$ instead of n because in the box beam analysis the space between the top and bottom covers is considered as a lamina with zero material properties. This allows for a common numbering sequence to be used throughout the depth of the beam and allows for the analysis of beam plates where the top and bottom covers are simply joined together.

The z_k are functions of y and are given in Ref. 6. Note that the A, B, and D matrices as used in this study differ from those used in the Classical Lamination Theory due to the fact that an integration over the y-coordinate is performed in this study to take into account the curvature of the top and bottom skins of the wing. In that sense, the present developments may be considered to be similar to those given by Giles[7] towards an equivalent plate analysis for laminated box wings using the Rayleigh-Ritz method.

The plate resultants N_y and M_y may be equated to zero, consistent with the beam theory assumptions neglecting the lateral stresses σ_y[5, 8]

$$N_y = A_{12}\epsilon_x^0 + A_{22}\epsilon_y^0 + A_{26}\gamma_{xy}^0 + B_{12}\kappa_x^w + B_{22}\kappa_y + B_{26}\kappa_{xy} + YA_2\kappa_x^v = 0 \tag{12a}$$

$$M_y = B_{12}\epsilon_x^0 + B_{22}\epsilon_y^0 + B_{26}\gamma_{xy}^0 + D_{12}\kappa_x^w + D_{22}\kappa_y + D_{26}\kappa_{xy} + YB_2\kappa_x^v = 0 \tag{12b}$$

However, the in-plane strain ϵ_y^0 and the bending curvature k_y are assumed to be nonzero. Solving the above equations simultaneously for ϵ_y^0 and k_y, the following expressions are obtained

$$\epsilon_y^0 = \frac{1}{\left(\frac{B_{22}^2}{D_{22}} - A_{22}\right)} \left[\left(A_{12} - \frac{B_{22}B_{12}}{D_{22}}\right)\epsilon_x^0 + \left(A_{26} - \frac{B_{22}B_{26}}{D_{22}}\right)\gamma_{xy}^0 + \left(B_{12} - \frac{B_{22}D_{12}}{D_{22}}\right)\kappa_x^w + \left(B_{26} - \frac{B_{22}D_{26}}{D_{22}}\right)\kappa_{xy} + \left(YA_2 - \frac{B_{22}YB_2}{D_{22}}\right)\kappa_x^v \right] \tag{13a}$$

$$k_y = \frac{1}{\left(\frac{B_{22}^2}{A_{22}} - D_{22}\right)} \left[\left(B_{12} - \frac{B_{22}A_{12}}{A_{22}}\right)\epsilon_x^0 + \left(B_{26} - \frac{B_{22}A_{26}}{A_{22}}\right)\gamma_{xy}^0 + \left(D_{12} - \frac{B_{22}B_{12}}{A_{22}}\right)\kappa_x^w + \left(D_{26} - \frac{B_{22}B_{26}}{A_{22}}\right)\kappa_{xy} + \left(YB_2 - \frac{B_{22}YA_2}{A_{22}}\right)\kappa_x^v \right] \tag{13b}$$

N_y and M_y can now be eliminated from the constitutive relations to obtain

$$\begin{bmatrix} N_x \\ N_{xy} \\ M_x^w \\ M_{xy} \\ M_x^v \end{bmatrix} = \begin{bmatrix} A_{11} & A_{16} & B_{11} & B_{16} & YA_1 \\ A_{16} & A_{66} & B_{16} & B_{66} & YA_6 \\ B_{11} & B_{16} & D_{11} & D_{16} & YB_1 \\ B_{16} & B_{66} & D_{16} & D_{66} & YB_6 \\ YA_1 & YA_6 & YB_1 & YB_6 & YD \end{bmatrix} \begin{Bmatrix} \epsilon_x^0 \\ \gamma_{xy}^0 \\ \kappa_x^w \\ \kappa_{xy} \\ \kappa_x^v \end{Bmatrix} + \begin{bmatrix} A_{12} & B_{12} \\ A_{26} & B_{26} \\ B_{12} & D_{12} \\ B_{26} & D_{26} \\ YA_2 & YB_2 \end{bmatrix} \begin{Bmatrix} \epsilon_y^0 \\ \kappa_y \end{Bmatrix} \tag{14}$$

where ϵ_y^0 and κ_y are given in terms of the remaining strains by Eqs. (13).

The transverse shear deformation is included in this formulation by splitting the transverse deflection in two parts:[8]

$$w = w_b + w_s \tag{15}$$

The w_s is evaluated following Timoshenko's method in which the transverse shear force-strain relation is the same as that used in Refs. 5 and 8.

Stringers' and Webs' Contribution

A stringer can be positioned at each of the eight sections, nodal lines running spanwise from one end of the element to the other end. The stringers are defined by their moduli E_i and cross-sectional areas, A_i. They are assumed to carry the axial stress σ_x only. Consequently, the terms defined in the previous sections are modified as given in Ref. 6. A shear web can be positioned between the top and bottom nodes of each of the four pairs of section nodes running along the length of the element. Each web is defined by its thickness h_i and shear modulus G_i and is assumed to carry transverse shear stresses τ_{xz} only. The transverse shear stiffness can be easily modified by the presence of webs.

Warping Correction Factor

Timoshenko's theory of beams neglects the axial restraint effects introduced by a clamped root. A cantilevered beam is not free to assume its normal deformed shape, and plane sections no longer remain plane under deformation. The shear-stress distribution is modified, and the torsional stiffness is increased. These effects vanish away from the root, but several studies by Crawley and Dugundji et al.[9,10] have shown that the decay length can be much larger for composite beams than for isotropic ones. In order to take these effects into account, the torsional stiffness term in the constitutive relations is multiplied by the warping correction factor $\kappa_{\ell t}$ defined by Crawley and Dugundji.[9] The warping correction factor is a function of both the material properties and the beam geometry and goes to 1 as the beam aspect ratio increases.

The strain energy expression for an element of length ℓ is given as

$$U = \frac{1}{2}\int_0^{\ell} \{\epsilon\}^t\{N\}dx \tag{16}$$

The details of the rest of the formulation of the various element matrices is quite standard, and thus it is not being given here. The details can be found in Ref. 6. It should be noted that a static condensation technique was used at the element level to reduce the number of degrees of the element from 24 to 12 by retaining only the degrees of freedom for w_b, w_s, and the twist angle τ at each node.

A coordinate transformation was used to account for different sweep angles for different segments of the wing.

Aeroelastic Model

The aerodynamic strip theory as developed by Barmby et al.[11] and modified by Yates[12] to account for finite span effects is used. The wing is divided in strips oriented normal to the spanwise axis and is assumed to undergo infinitesimal harmonic oscillations about its steady-state position. Chordwise camber effects are neglected so that the relevant displacements are the twist angle τ and the vertical deflection of the reference line w. The aerodynamic loads are resolved as a lift L, positive up, acting at the aerodynamic center, and a moment M about the reference line positive leading edge up.

Finite span effects are accounted for by replacing the two-dimensional values of a_c, the nondimensional offset between aerodynamic center and semichord line, and $C_{\ell\alpha}$, the lift curve slope, by steady-state values obtained from any suitable method, as for example the Weissinger L-method.

Assuming sinusoidal motion of frequency ω:

$$w(x,t) = w(x)e^{i\omega t}, \qquad \tau(x,t) = \tau(x)e^{i\omega t} \tag{17}$$

the aerodynamic loads are from Ref. 13:

$$L = \rho\omega^2[L_w w + L_\tau \tau + L_\theta \theta + L_{\tau'}\tau'] \tag{18a}$$

$$M = \rho\omega^2[M_w w + M_\tau \tau + M_\theta \theta + M_{\tau'}\tau'] \tag{18b}$$

where $\theta = \frac{dw}{dx}$ and ρ = air density. The variables L_w, L_τ, L_θ, L_τ, M_w, M_τ, M_θ and M_τ are given in Ref. 13.

The displacements $w = w_b + w_s$, θ, τ, τ' may be expressed as functions of the reduced nodal displacement vector in terms of Hermitian Polynomials and their derivatives: $w = N_w^t\{q\}$ and similarly for θ, τ and τ'. Thus

$$L = \omega^2\{L_w N_w^t + L_\theta N_\theta^t + L_\tau N_\tau^t + L_{\tau'} N_{\tau'}^t\}\{q\} \tag{19}$$

$$M = \omega^2\{M_w N_w^t + M_\theta N_\theta^t + M_\tau N_\tau^t + M_{\tau'} N_{\tau'}^t\}\{q\} \tag{20}$$

To derive the aerodynamic matrix, we express the nonconservative virtual work due to the distributed aerodynamic loading along the span of the element:

$$\delta W = \int_0^{\ell} \delta w L dx + \int_0^{\ell} \delta\tau M dx \tag{21}$$

$$\{\delta q\}^t[\int_0^{\ell} (L_w N_w N_w^t + L_\theta N_w N_\theta^t + L_\tau N_w N_\tau^t + L_{\tau'} N_w N_{\tau'}^t \tag{22}$$

$$+ M_w N_\tau N_w^t + M_\theta N_\tau N_\theta^t + M_\tau N_\tau N_\tau^t + M_{\tau'} N_\tau N_{\tau'}^t)^2 dx]\{q\}$$

$$= \{\delta q\}^t\omega^2[a]\{q\} \tag{23}$$

Thus the nodal load vector equivalent to the distributed aerodynamic loading is $\omega^2[a]\{q\}$ where $[a]$ is the complex element aerodynamic matrix.

The integration of the aerodynamic matrix follows the Gaussian quadrature. Note that the aerodynamic matrix is not symmetric.

The equations of motion of the wing oscillating in unsteady flow are

$$([K] - [M]\omega^2 - [A]\omega^2)\{q\} = \{0\} \tag{24}$$

where $[A]$, the assembled aerodynamic matrix, is a function of the flow speed V through the reduced frequency $k = \frac{\omega b_r}{V}$. These equations are solved for the flutter speed and frequency using the familiar V-g method. Divergence can also be obtained from the V-g method. It is characterized by the structural damping of a mode going abruptly from a negative value to zero (without crossing the V-axis) at the same time the frequency goes to zero. This is obtained for a very low value of the reduced frequency k.

Alternatively, the divergence speed V is obtained by setting the mass matrix and the time-dependent terms of the aerodynamic matrix to zero and solving the equations of motion. The corresponding eigenvalue problem is

$$\{[A_{\text{stat}}] - \lambda[K]\}\{q\} = 0 \tag{25}$$

where $[A_{\text{stat}}]$ is now real and $\lambda = 1/V^2$. The largest positive eigenvalue yields the divergence speed of the wing.

Numerical Results

Evaluative Analysis

This section presents the results obtained by the present element for a number of problems found in the literature. The evaluation process was divided in four phases to validate successively all components of the model. Several static deflection

cases were first analyzed to check the stiffness matrix. The mass matrix formulation was then verified by solving problems in free vibrations. Having gained confidence in the structural model, attention was focused on the divergence speed of straight, forward, and swept-back wings. Finally, the solution procedure and the dynamic aerodynamic matrix were evaluated by performing a number of flutter calculations on wings for which alternative results were available.

Static Response of Builtup Double Swept Wing

In addition to a number of simple problems, the capability of the present development for solving static problems was evaluated by analyzing a complex structure representative of current forward swept designs. The wing is shown in Fig. 2, and it features double sweep, both chord and thickness tapers, and unsymmetrical top and bottom shapes and laminations. It includes four webs and eight stringers. The top and bottom skins are made of layers of graphite/epoxy ($E_1 = 19.0 \times 10^6$ psi, $E_2 = 1.89 \times 10^6$ psi, $v_{12} = 0.38$, $G_{12} = 0.93 \times 10^6$ psi) oriented at 0, 90, +45 and −45 deg. The thickness of each layer varies in each segment in the wing.

The wing was subjected to a vertical tip load and the tip deflection obtained by two different methods: the present formulation and WIDOWAC[14] were compared. The WIDOWAC model uses rod, shear-web, and triangular membrane elements. The present one-dimensional model, shown in Fig. 3, uses eight elements to account for the changes in sweep, taper, and skin thickness along the span. For this study, orientation of the laminates constituting the covers was varied from 0 to 180 deg. relative to the spanwise axes of each element. This was achieved by assigning the same design variable to the orientation of all laminas.

The tip deflection is plotted against the cover orientation in Fig. 4. Note that the boundary conditions for the two models are different: the root and tip of the WIDOWAC model are parallel to the airstream. The present formulation, on the other hand, is one-dimensional and therefore assumes an effective root and tip perpendicular to the midchord line. The agreement shown in Fig. 4 is nevertheless found to be very good.

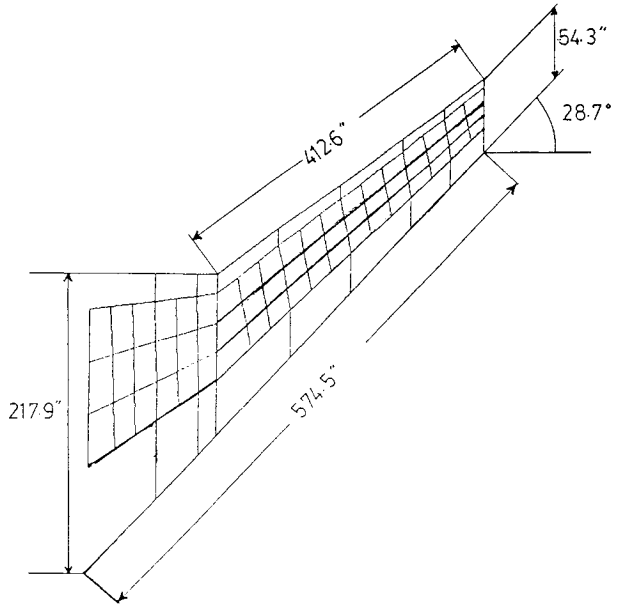

Fig. 2 Builtup double swept wing geometry.

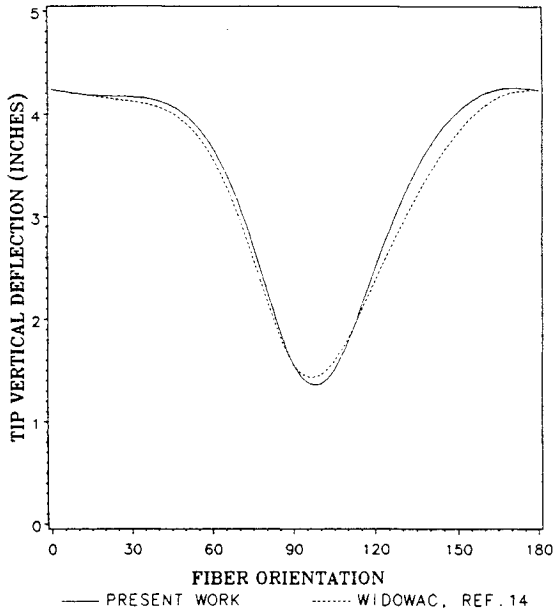

Fig. 4 Tip deflection of a builtup wing under tip load.

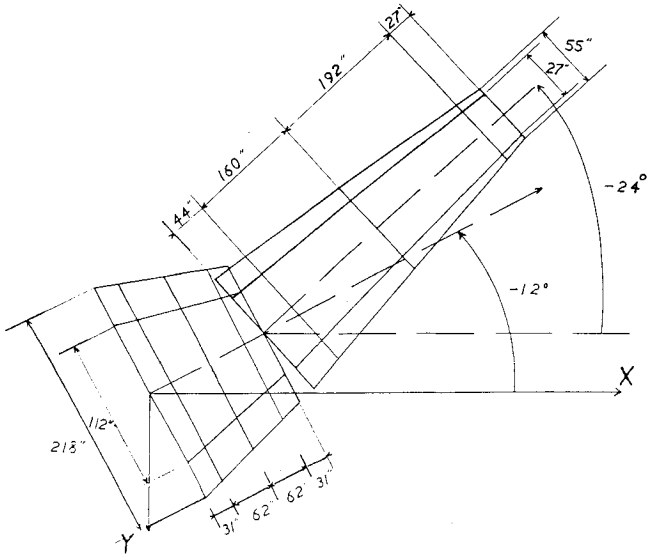

Fig. 3 Builtup wing model for the present work.

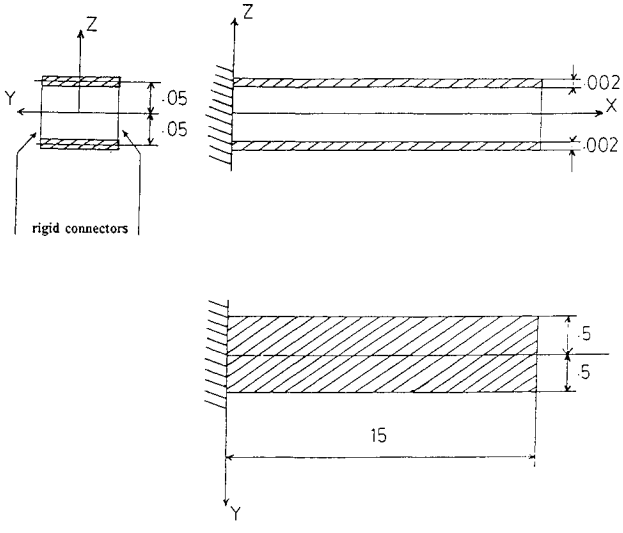

Fig. 5 Box beam geometry.

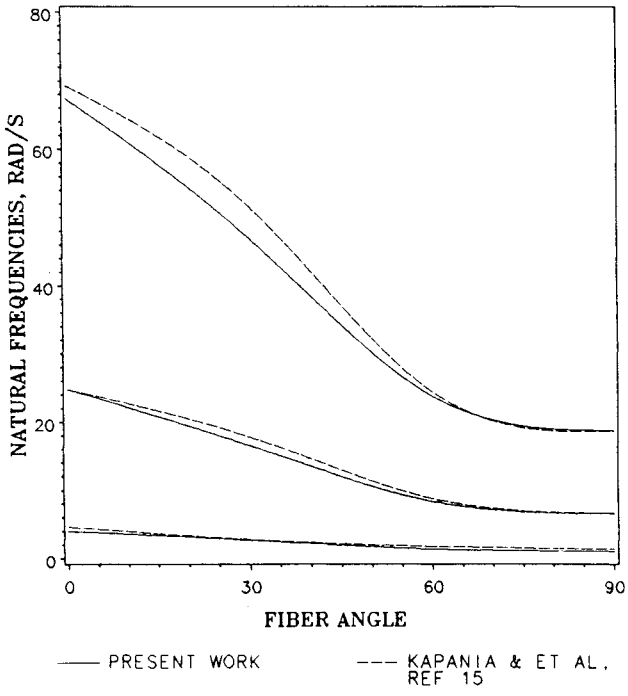

Fig. 6 Natural frequencies of a box beam.

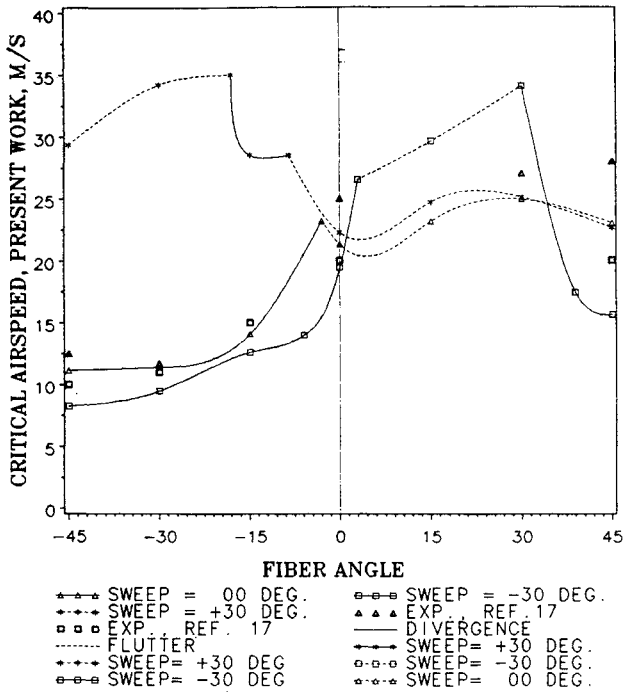

Fig. 7 Flutter and divergence speeds of swept graphite/epoxy plates.

Free Vibration Analysis

A number of test examples were studied to evaluate the performance of this element to obtain the free vibration response. These test examples included 1) a unidirectional Graphite/Epoxy Cantilever beam, 2) rectangular symmetrically laminated cantilever plates, 3) unsymmetrically laminated square plate, and 4) a box beam shown in Fig. 5. For all these examples, the results obtained using the present formulation were found to be in good agreement with those available in the literature. For example, Fig. 6 shows the comparison of the first three natural frequencies obtained by Kapania, Bergen, and Barthelemy[15] and the present formulation using four elements. The results in Ref. 15 were obtained using the Equivalent Plate Model program developed by Giles.[7]

Divergence and Flutter

Attention was next turned to the evaluation of the aerodynamic matrix. The evaluative examples included 1) divergence of swept isotropic wings for which alternative results were available, 2) divergence and flutter of swept wings for which analytical and experimental results were given by Barmby, Cunningham and Garrick,[11] 3) divergence and flutter of Graphite/Epoxy laminated cantilever plates for which analytical and experimental results were given by Hollowell and Dugundji[16] and by Landsberger and Dugundji,[17] and 4) divergence and flutter of box beams for which analytical results were obtained by Kapania, Bergen and Barthelemy.[15] For all the examples considered, good agreement was obtained between the present results and those obtained by other investigators. Figure 7, for instance, shows the summary of the results obtained in this study for the unswept, 30-deg swept forward and 30-deg swept-back plates. The present results were found to be in good agreement with those given in Ref. 17. For more details, the reader is referred to Ref. 6.

Aeroelastic Properties of Unsymmetric and Damaged Wings

Most studies on the aeroelastic response of laminated wings are limited to structures having a plane of symmetry perpendicular to the thickness direction. In that case, the $[B]$ matrix from Classical Lamination Theory is zero and flexure and extension are decoupled, thereby greatly simplifying the analysis. Actual designs, however, are not in general symmetric. In addition, damage to the structure caused by fatigue, manufacturing defects, or impact is unlikely to occur in a symmetric fashion. The behavior of an initially symmetric structure is thus going to be modified by both the lower stiffness and the presence of bending-stretching coupling. In this section, the capability of the present formulation to analyze unsymmetric structures is exploited to study the influence of the B_{ij} coupling terms on the aeroelastic response of a laminated beam.

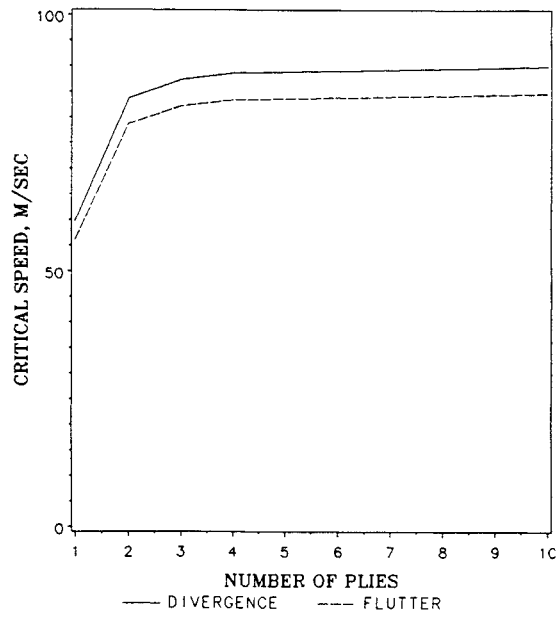

Fig. 8 Flutter and divergence speeds of an angle ply laminate.

Angle Ply Beam-Plate

The purpose of this section is to investigate the influence of the coupling term B_{16}. A beam having a rectangular solid cross section and a lamination sequence of $[(+45/-45)_n]$ has been chosen, where the total thickness of the beam is kept constant as n is varied.

The rectangular uniform beam having the following properties is used: $E_1 = 6.9 \times 10^{10}$ N/m^2, $E_2 = 5.0 \times 10^9$ N/m^2, $\nu_{12} = 0.30$, $G_{12} = 1.5 \times 10^{10}$ N/m^2, $\rho = 2.71 \times 10^3$kg/m^3, $\ell = 1.5$ m, $b = .1$ m, h = 0.0049 m. The sweep angle is set to zero. Note that in this case the D_{16} and D_{26} are zero. The divergence and flutter speeds are shown in Fig. 8. It is seen that for $n = 1$, which yields the highest value for B_{16}, the critical speeds are down to 66% of their symmetric values but that the ratio converges very rapidly towards 1 as n increases.

Angle Ply Forward Swept Box Beam

One of the most important aerospace applications of fiber reinforced materials is the tailoring of forward swept wings for divergence elimination. Only one such design is flying today, and very little information is available concerning the damage tolerance of composite forward swept wings. As a first step, it is of interest to investigate the influence of asymmetry on the aeroelastic response of such wings. For this purpose, the previously defined box beam (see Fig. 5) was swept at a 30 deg forward angle and assigned a $[\theta/(+45/-45)_n/\theta]$ stacking sequence. The total thickness of the skins was kept constant as n was varied. Prior to varying n, a wing having similar bending stiffnesses, with a symmetric lamination sequence of $[\theta/+45/-45/-45/+45/\theta]$, was aeroelastically tailored for divergence. The maximum divergence speed was obtained for $\theta = 36$ deg. This value of θ was then kept constant, and the value of n increased. Table 1 presents results for B_{16}, EI_{eq}, GJ_{eq}, K_{eq}, and (Vd/V_{ref}), where K_{eq} is the bending-torsion coupling term which is the cornerstone of aeroelastic tailoring, and V_{ref} is the divergence speed of the symmetric wing for $\theta = 0$ deg. A striking result is the large increase in divergence speed when a high bending-stretching coupling is present. The examination of the equivalent stiffnesses[6] for this case reveals only a modest increase for K_{eq} and small decreases for EI_{eq} and GJ_{eq}, but divergence elimination is a phenomenon known to vary greatly for slight changes in fiber orientation. This result suggests that asymmetry might be a design option for forward swept wings. As in the previous section, the influence of B_{16} vanishes rapidly when n is increased.

Table 1 Aeroelastic response of a [36/(45/−45 deg)$_n$/36 deg] forward swept angle ply box beam

n	V_d/V_{ref}	EI_{eq} (N.m^2)	GJ_{eq}(N.m^2)	K_{eq}(N.m^2)	B_{16}(N)
1	35.0	848,356.	207,269.	254,471.	776,440.
2	3.0	855,139.	225,785.	244,602.	2011.
3	2.01	855,139.	225,593.	244,465.	0.

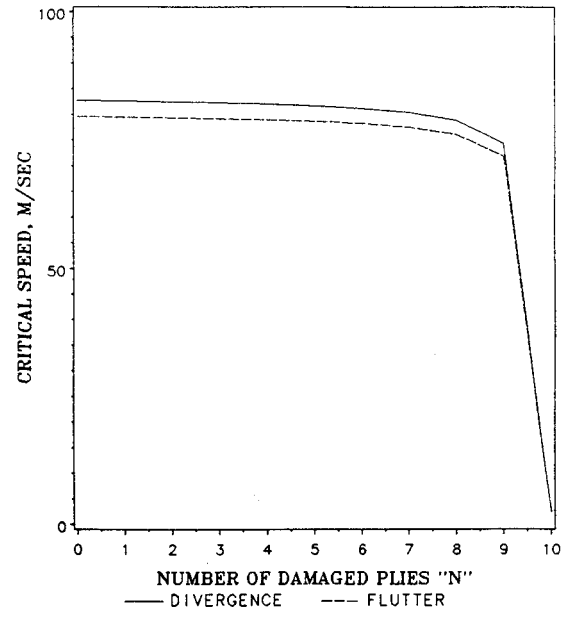

Fig. 9 Flutter and divergence speeds of a damaged box beam.

Damaged Unswept Box Beam

The influence of damage on the aeroelastic response of an unswept box beam having the same geometry and material properties as in the previous section was next studied. The cover skins are unidirectional, the fibers being oriented parallel to the spanwise axis ($\theta = 0$ deg). Both top and bottom skins are made of ten layers of equal thickness. The beam is modeled using six elements, and damage is applied to the top skin of the next to last element (going towards the tip). This location was found by Eastep et al.[4] to be critical for flutter. The damage was modeled as a complete loss of stiffness for the corresponding layers. The mass and geometry of the structure was assumed to remain unchanged. In particular, the aerodynamic loads retain their undamaged values. This modeling is therefore not adequate for analyzing that impact induced damage for which the airfoil shape, and therefore the aerodynamic loads, would be modified. It is also not possible to simulate damage to only the inner plies of the skin or due to delamination. In that case, the remaining layers above and below the damaged plies would act as distinct entities. Such a behavior was modeled by Kapania and Wolfe.[18] Figure 9 presents the divergence and flutter speeds of the beam as functions of the number of damaged layers. Once again, the influence of the bending-extension coupling introduced by the damage induced unsymmetry vanishes rapidly as the unsymmetry decreases. In the present case, however, when the entire top cover is damaged this coupling causes the stiffnesses to go to very low values, yielding zero divergence and flutter speeds.

For comparison purposes, damaging the wing in a symmetric fashion to obtain the same decrease for $[A]$ and $[D]$ but no $[B]$ terms yielded a decrease in divergence speed of 2.3%, and the flutter speed decreased by 2.1%. Unsymmetry is thus seen to have important effects on the aeroelastic response of damaged composite wings.

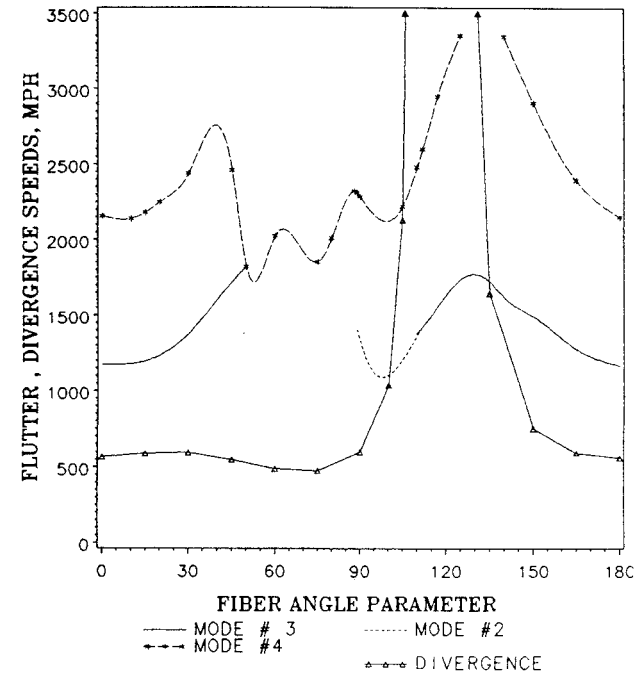

Fig. 10 Flutter and divergence speeds of a builtup double swept wing.

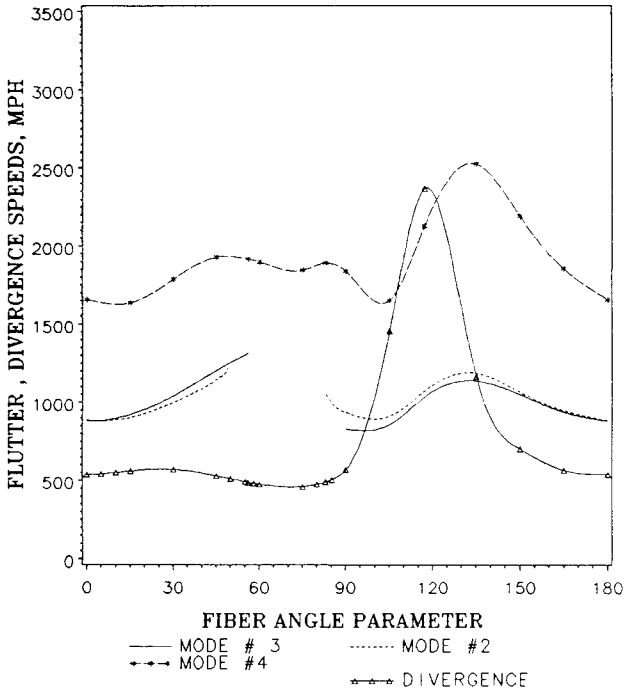

Fig. 11 Flutter and divergence speeds of a damaged builtup wing, first case.

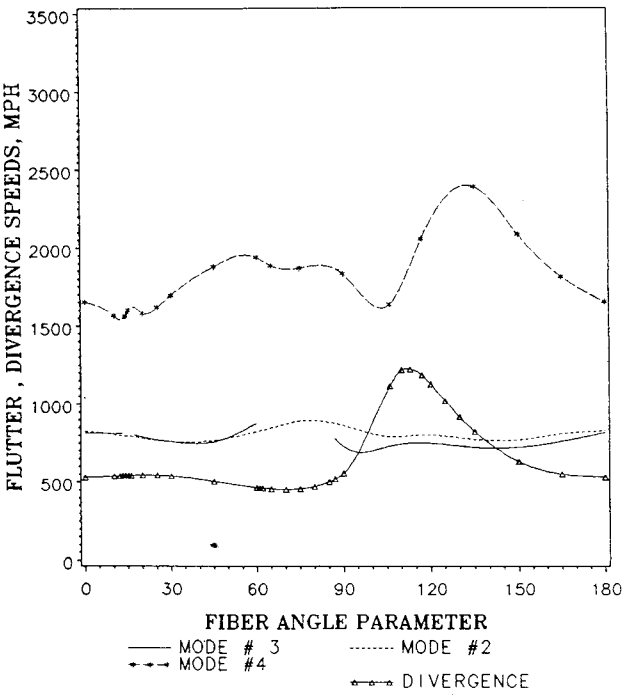

Fig. 12 Flutter and divergence speeds of a damaged builtup wing, second case.

Undamaged and Damaged Builtup Wing

Finally the aeroelastic behavior of the double swept wing described previously (see Figs. 2–4) was studied. This wing features top and bottom cover skins of different curvatures and thicknesses and top and bottom stringers of different size. It is thus strongly unsymmetric.

For this study, a common design variable was assigned to all laminae of the top and bottom cover skins of all the elements. This design variable, a convenient parameter to study the tailoring effects, was then varied from 0–180 deg, and the divergence and flutter speeds obtained for all orientations. It should be pointed out, however, that this variable is not an actual orientation angle but rather an "orientation parameter." The cover skins are made of a combination of 0, 90 and $+/-45$ deg plies, and have different initial orientation angles in each element.

Figure 10 shows the aeroelastic response of the undamaged wing. Of interest is the range of angles around 120 deg for which divergence is eliminated. The (current) actual design for this wing calls for a design variable value of 117 deg. It is seen that outside this narrow range, divergence is more critical than flutter. Also noteworthy is the sudden switch in flutter mode for $\theta = 85$ deg.

Effect of Damage

Having obtained the initial response of the wing, a damage study was performed. The location of the damage is the same as in the previous section. The cover at this point is made of a thick (= .3 in.) 90-deg ply and thin (= .05 in.) $+/-45$-deg and 0-deg plies. Note that $\theta = 117$ deg places the strongest direction of the 90-deg ply between 10 and 30 deg forward of the wing axis, which is known to be the optimum position for divergence elimination.

Two damage cases were studied, where 90% (case 1) and 100% (case 2) of the 90 deg ply were damaged. Results are shown for flutter and divergence in Fig. 11 for case 1 and in Fig. 12 for case 2. The trends revealed in the previous sections are again apparent here, the wing's aeroelastic response being affected when a very high bending-extension coupling is present. Also note that the flutter speed is affected more than the divergence speed for untailored configurations, that is, when the fiber angle parameter θ is outside of the interval 110 deg–140 deg for which divergence is eliminated. Within this interval, however, damage is seen to weaken the divergence elimination capacity.

Concluding Remarks

A simple element for the aeroelastic analysis of laminated wings has been developed. The formulation allows for unsymmetric laminations, arbitrary geometry including chord and thickness taper, and multiple sweep angles. The formulation and computer program have been evaluated by solving problems found in the literature. The element provides an efficient tool for the rapid analysis of a wide range of aeroelastic structures.

The capacity of the element to analyze unsymmetrically laminated structures was exploited by studying the influence of bending-extension coupling on the aeroelastic response of composite wings. It was found that this coupling lowers the bending and torsional stiffnesses but may in some cases increase the bending-torsion interaction which allows for aeroelastic tailoring of composite lifting surfaces. It is thus possible to enhance the aeroelastic performance of such structures by introducing unsymmetry in the design. Unsymmetry due to damage, however, was shown to have a detrimental effect for the wings investigated because of a simultaneous drop in the extensional, bending, and bending-extension stiffnesses.

Limitations of the present model should be kept in mind. The torsional stiffness of the wing is assumed to be provided only by the top and bottom covers. This neglects the axial stress system induced in the axially restrained stringers by the torsional deformations. The contribution of the webs is also neglected. Also, the present one-dimensional model may not account properly for the stress distribution and load transfer mechanisms in the different components of the damaged builtup structure.

Acknowledgments

We would like to thank Drs. R.T. Haftka and E.R. Johnson for their suggestions and comments, Dr. J.A. Schetz, Department Head, Aerospace and Ocean Engineering, VPI & SU and

NASA Langley Research Center (Grant No. NAG-1-168 with R.T. Haftka as Principal Investigator) for providing partial financial support.

References

[1]Krone, N. J., "Divergence Elimination with Advanced Composites," AIAA Paper 75-1009.

[2]Weisshaar, T. A., "Divergence of Forward Swept Composite Wings," *Journal of Aircraft,* Vol. 17, June 1980, pp. 442-448.

[3]Eastep, F. E., Venkayya, V. B., and Tishler, V. A., "Divergence Speed Degradation of Forward Swept Wings with Damaged Composite Skin," *Journal of Aircraft,* Vol. 21, No. 11, Nov. 1984, pp. 921-923.

[4]Starnes, J. H., Jr. and Haftka, R. T., "Preliminary Design of Composite Wing-Box Structures for Global Damage Tolerance," *Proceedings of the 21st AIAA Structures, Structural Dynamics and Materials Conference,* Professor, AIAA, Washington, DC, May 1980.

[5]Kapania, R. K. and Raciti, S., "Nonlinear Vibrations of Unsymmetrically Laminated Beams," AIAA Paper 87-CP-0859 also *AIAA Journal,* Vol. 27. No. 2, Feb. 1989, pp. 201-210.

[6]Castel, F. and Kapania, R. K., "A Beam Element for Aeroelastic Analysis of Damaged and Undamaged Laminated Wings," *Center for Composite Materials and Structures,* CCMS-88-13, Virginia Polytechnic Institute and State University, Blacksburg, VA, 1988.

[7]Giles, G. L., "Equivalent Plate Analysis of Aircraft Wing Box Structures with General Planform Geometry," NASA TM 87697. March 1986.

[8] Chen, A. T. and Yang, T. Y., "Static and Dynamic Formulation of a Symmetrically Laminated Beam Finite Element for a Microcomputer," *Journal of Composite Materials,* Vol. 19, 1985, pp. 485-49.

[9] Crawley, E. F. and Dugundji, J., "Frequency Determination and Nondimensionalization for Composite Cantilever Plates," *Journal of Sound and Vibrations,* Vol. 72, No. 1, Sept. 1980, pp. 1-10.

[10]Jensen, D. W., Crawley, E. F., and Dugundji, J., "Vibration of Cantilevered Graphite/Epoxy Plates with Bending/Torsion Coupling," *Journal of Reinforced Plastics and Composites,* Vol. 1, July 1982, pp. 254-261.

[11]Barmby, J. G., Cunningham, H. J., and Garrick, I. E., "Study of Effects of Sweep on the Flutter of Cantilever Wings," NACA TN-2121, June 1950.

[12]Yates, E. C., Jr., "Modified-Strip-Analysis Method for Predicting Wing Flutter at Subsonic to Hypersonic Speeds," *Journal of Aircraft,* Vol. 3. No. 1, Jan. 1966, pp. 23-27.

[13]Yates, E. C., Jr., "Calculation of Flutter Characteristics for Finite-Span Swept or Unswept Wings at Subsonic and Supersonic Speeds by a Modified Strip Analysis," NACA RM L57L10, 1958.

[14]Haftka, R. T., "Automatic Procedure for the Design of Wing Structures to Satisfy Strength and Flutter Requirements," NASA TN D-7264, 1973.

[15]Kapania, R. K., Bergen, F., and Barthelemy, J. F. M., "Sensitivity Analysis of a Flutter Response of a Laminated Wing," AIAA-Paper-CP89-1267.

[16]Hollowell, S. J. and Dugundji, J., "Aeroelastic Flutter and Divergence of Stiffness Coupled Graphite/Epoxy Cantilevered Plates," AIAA Paper 82-0722.

[17]Landsberger, B. J. and Dugundji, J., "Experimental Aeroelastic Behavior of Unswept and Forward Swept Cantilever Graphite/Epoxy Wings," Journal of Aircraft, Vol. 22, No. 8, August 1985, pp. 679-686.

[18]Kapania, R. K. and Wolfe, D. R., "Delamination Buckling and Growth in Axially Loaded Beam Plate," AIAA Paper 87-0878-CP.